Canadian Conference - Pacific Conference on Earthquake Engineering 2023
Vancouver, British Columbia
June 25th – June 30th, 2023

Seismic Behavior Assessment of Fe-SMA-based Buckling-restrained Braced Frames

Subhrajyoti Jena[1*], Deepak Yadav[2], Dipti Ranjan Sahoo[3], K. Eugene Kim[4]

[1]Research Scholar, Department of Civil Engineering, Indian Institute of Technology Delhi, New Delhi, India
[2]Post-doctoral Fellow, Department of Civil Engineering, Indian Institute of Technology Delhi, New Delhi, India
[3]Professor, Department of Civil Engineering, Indian Institute of Technology Delhi, New Delhi, India
[4]Assistant Professor, Department of Civil and Environmental Engineering, University of Waterloo, Ontario, Canada
[*]subhrajyotijena1298@gmail.com (Corresponding Author)

ABSTRACT

The use of Shape Memory Alloy (SMA) in Buckling-restrained Braces (BRBs) improves its self-centering capacity resulting in excellent energy dissipation with lower residual drifts of structures. The current study uses the cost-efficient iron-based SMA (Fe-SMA) as the core material of BRBs exploiting the super-elasticity and high post-yield stiffness of Fe-SMA to reduce the residual deformation of the brace. The study involves the assessment of the hysteretic performance of Fe-SMA-based BRBs (FSBRB). A numerical model of FSBRB has been developed using OpenSees (OS) and validated based on test results. Further, the effect of using Fe-SMA as the core element in BRBs has been investigated by performing a set of nonlinear time history analyses of steel-braced frames. The braces used in the study use FSBRB connected to a tubular section in series. The tubular section has been designed to remain in the elastic range for the expected deformation demand. Obtained results are compared with those obtained from seismic analysis of frames designed with conventional BRBs.

Keywords: Buckling-restrained braces, Fe-SMA, Hysteretic response, Energy dissipation, Residual drift

INTRODUCTION

The design of buildings using Buckling-restrained braces (BRBs) to mitigate the excess drift originating due to a seismic event has gained popularity over the years in various countries such as the United States, New Zealand, Canada, China, and Japan, among others, starting from the late 1980s [1]. Buckling-restrained mechanism of BRBs results in stable hysteretic energy dissipation capacity for both tension and compression loading cycles and hence offers better seismic performance over traditional bracing systems [2]. Though, the significant residual story drifts associated with the buildings designed with BRBs as lateral force-resisting systems after an earthquake can severely affect their reusability and the repairing costs [3,4].

The researchers have suggested various methods to minimize the residual drifts associated with BRB systems having similar energy dissipation capacity over the years. The higher post-yield stiffness of the system can reduce the residual story drifts, as suggested by Macrae et al. [5]. The use of dual frame systems incorporating both moment-resisting frames (MRFs) and buckling restrained braced frames (BRBFs) [6] increases the post-yield stiffness of the system, which reduces the residual drifts of the structures. Another technique to minimize the residual story drifts involves the use of self-centering BRBs, which provides the restoring force to the system. The restoring forces can be provided by using post-tensioning tendons [7,8] or using shape memory alloys (SMA) [9]. SMA has unique properties by virtue of which it can return to its original configuration upon heating (shape memory effect) or unloading (super-elastic effect) the element [10]. Miller et al. [9] experimentally investigated the effect of using pre-stressed Nickel-Titanium-based SMA (Nitinol) rods placed between concentric tubes, ensuring parallel connection with the BRBs. These SMA rods possessing the unique super-elastic property along with the initial pre-stressing resulted in reduced residual drifts of the system, as confirmed by the subsequent studies [11,12]. Issa et al. [13] conducted experimental and numerical studies of bracing systems utilizing the SMA for energy dissipation and recentering mechanism. Most previously mentioned studies have been conducted using costlier Nickel-Titanium based SMAs. Iron (Fe) based SMA (Fe-SMA) can be a cost-effective alternative to Nitinol for designing BRBs utilizing SMA as the energy-dissipating element. Ghowsi et al. [14] studied the hysteretic behavior of hybrid BRBs, which utilizes the Fe-SMA as the core element representing the yielding part of the brace. The length of the core element was kept between 14-25% of the work point-to-work point length to minimize the fabrication cost. The selection of a shorter length of core element enhances the axial stiffness and strain-hardening factor owing to higher strain demands, which can help mitigate the higher residual drifts associated with the conventional BRBs [15,16]. The study conducted by Hoveidae et al. [17] showed that the short-core BRBs comprising stainless steel with high strain-hardening behavior led to a considerable reduction in residual drifts. As the core material is subjected to high strain demands owing to shorter core lengths, the core region comprising Fe-SMA can be a better option considering the excellent fatigue characteristics of Fe-SMA [10]. Qiu et al. [18] investigated the seismic performance of three and six-story buildings utilizing three different types of Fe-SMA as the core element and compared the results with conventional BRBF systems. However, the effect of using such Fe-SMA BRBs (FSBRB) in reducing story drifts still needs to be studied for their application in mid-rise and high-rise structures.

The present study focuses on predicting the seismic response of 3-story, 6-story, and 9-story frames designed using short-core hybrid FSBRBs subjected to a set of ground motions representing the design basis earthquake (DBE) hazard level. The numerical modeling of the FSBRB specimen has been performed using OpenSees [19]. The main parameters investigated are maximum inter-story and residual drifts of the structures. The effect of post-yield stiffness of FSBRBFs in the reduction of residual drifts has been compared with equivalent steel BRBFs.

CONCEPT OF HYBRID FSBRB

The configuration of the hybrid FSBRB used in the current study is similar to the one used by Ghowsi et al. [14]. The bracing system consists of a Fe-SMA-based core element, which is connected to the tubular section in series, as shown in Figure 1. The HSS section is designed to remain elastic under the application of axial loading, considering the expected overstrength resulting due to strain-hardening. The current study involves the use of Fe-28Mn-6Si-5Cr SMA as the core element which belongs to the group of Fe-Mn-Si SMAs possessing excellent low-cycle fatigue performance, high post-yield stiffness ratio, and good machining properties [10]. Figure 2 shows the typical force-deformation behavior of FSBRBs and steel BRBs having the same initial stiffness with different post-yield stiffness. The higher post-yield stiffness of FSBRBs results in lower zero-force residual deformation.

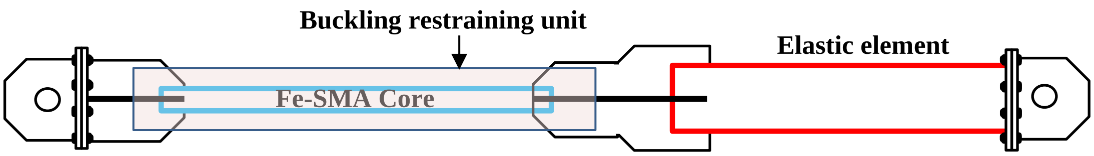

Figure 1. Schematic representation of a typical FSBRB specimen.

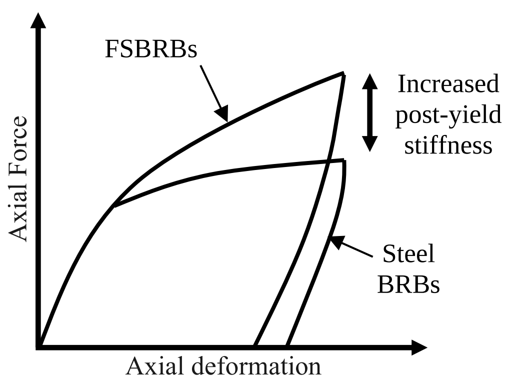

Figure 2. Schematic representation of force deformation behavior of FSBRB and Steel BRB systems.

DESIGN METHODOLOGY

Details of building models

The study focuses on the numerical investigation of seismic response of 3-story, 6-story, and 9-story office buildings assumed to be in Downtown, Los Angeles, belonging to the risk category II. The buildings have been assumed to be constructed on stiff soil belonging to the site classification category D. The design spectral response acceleration parameter in the short period range (S_{DS}) and 1.0s period (S_{D1}) is 1.51g and 1.11g, respectively, which has been computed using the online hazard tool of

ASCE. The floor dimensions and seismic masses have been adopted from the benchmark buildings based on SAC Phase-II steel projects [20]. The 3-story building consists of four and six bays of 9.15 m width each in both orthogonal directions with a constant floor height of 3.96 m (Figure 3 (a) and Figure 3 (c)). The 9-story building comprising five bays of 9.15 m width each in both directions has the same floor-to-floor height of 3.96 m except for the first story, which is equal to 5.49 m (Figure 3 (b) and Figure 3 (e)). The dimensions (plan) of the 6-story building have been considered to be the same as the dimensions of the 9-story building, as shown in (Figure 3 (b) and Figure 3 (c)). The perimeter frames of all the buildings are braced with steel and Fe-SMA BRBs such that there are four braced bays in each direction. The seismic weights of the 3-story, 6-story, and 9-story buildings are 28978.74 kN, 59213.16 kN, and 88319.43 kN, respectively. As shown in Figure 3 (c), Figure 3 (d), and Figure 3 (e), the braced frame along the shorter direction of the buildings have been considered for the modeling. The following six types of frames have been modeled: 3-story frames with BRB and Fe-SMA BRBs (BRBF3 and FSBRBF3), 6-story frames with BRB and Fe-SMA BRBs (BRBF6 and FSBRBF6), and 9-story frames with BRB and Fe-SMA BRBs (BRBF9 and FSBRBF9) frames.

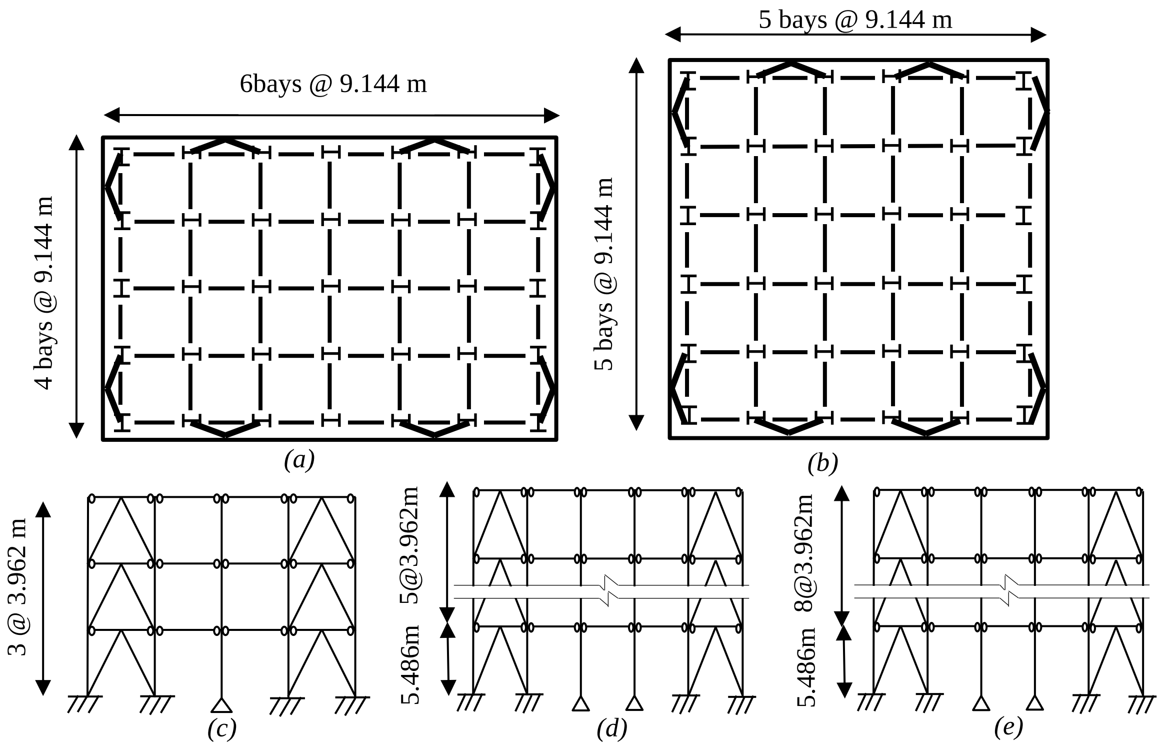

Figure 3. Dimension of the building: a) plan of 3-story, (b) plan of 6-story and 9-story, (c) 3-story elevation, (d) 6-story elevation, (e) 9-story elevation.

Preliminary design of the braced frame

The frames comprising steel and Fe-SMA BRBs were designed as per the Equivalent Lateral Force (ELF) method. For the preliminary sizing of the braces, the base shear value has been computed using the code-provided empirical formula for the approximate time period, T_a, calculated based on the height of the structure [21]. Thus, the values of T_a can be computed as:

$$T_a = C_t h_i^x \tag{1}$$

Where h_i represents the height of the structure, the value of C_t and x are 0.0731 and 0.75 for BRBs. The calculated values of T_a for 3-story, 6-story, and 9-story buildings are 0.468s, 0.825s, and 1.101s, respectively. The response reduction factor (R), deflection amplification factor (C_d), and overstrength factor (Ω_0) for BRBFs considered in the current study are based on the code-provided values of 8.0, 5.0, and 2.5, respectively.

Thus, the seismic design base shear, V. can be computed as:

$$V = C_s W \tag{2}$$

Where C_s is the base shear coefficient, and W is the seismic weight of the building. The design shear values of 3-story, 6-story, and 9-story buildings are 5469.74 kN, 9963.55 kN, and 11132.45 kN, respectively. The code-provided formula for the vertical distribution of forces has been considered for calculating the story seismic forces. As the bracing configuration considered in the studied buildings is symmetric in both directions, the seismic story forces have been distributed among the lateral load-resisting elements considering 5% accidental eccentricity. Based on these story forces, the axial force demand on the braces has been computed to determine the core area of the BRBs.

Braces are assumed to carry only the lateral load arising due to earthquakes. Hence the forces in the BRBs are computed, neglecting the effects of the gravity loads on the braces. The required core area of the BRBs is calculated as follows:

$$A_c = \frac{P_{bd}}{\phi F_{yc}} \tag{3}$$

Where P_{bd} is the design brace force considering second-order effects, ϕ is the strength reduction factor (equal to 0.9), F_{yc} is the yield stress of the core material of the BRB. For the Fe-SMA-based core material of BRBs, the yield stress and elastic modulus are 250 MPa and 170 GPa, respectively [10]. The yield stress of the steel core has been considered as 330 MPa [22].

Beams and columns are designed using the load combinations mentioned in the ASCE 7-16 [21], including the dead loads, live loads, and loads due to the expected strengths of the BRBs. The expected strength of the BRBs in tension is computed as the product of the tensile yield strength (P_{yc}), material over-strength factor (R_y), and strain-hardening adjustment factor (ω). Similarly, the expected strength of the BRBs in compression is obtained by multiplying the compression strength adjustment factor (β) with the expected tensile strength of the BRBs. The values of ω and β for the preliminary design of the frame elements have been assumed as 1.4 and 1.1, respectively [23]. The same values of ω and β have been considered in the current study for both steel and Fe-SMA-based BRBs to ensure the same section sizes of the beams and columns to better compare the global responses of the frames using these types of BRBs. It is noted that the value of ω will be higher for Fe-SMA BRBs considering the high post-yield stiffness of Fe-SMA BRBs. The beams and columns have been designed to satisfy the moderately ductile section limits provided in ANSI/AISC 341-16 [24]. The frames have been checked for the inelastic drift limits calculated using the deflection amplification factor and drift from the first-order elastic analysis. Table 1 shows the final member sizes and brace core areas for all six types of frames.

Table 1. Brace core area and frame section details used in the analysis.

	Story No.	**BRB area**	**FSBRB area**	**Braced Bays**		**Unbraced bays**	
		(mm^2)	**(mm^2)**	**Beams**	**Columns**	**Beams**	**Columns**
3-story	3rd Story	1774	2341	W14X132	W14X120	W12X96	W14X53
	2nd Story	2903	3832	W14X145	W14X120	W12X96	W14X68
	1st Story	3226	4258	W14X159	W14X132	W12X96	W14X74
6-story	6th Story	1935	2555	W14X132	W14X211	W14X53	W14X145
	5th Story	3226	4258	W14X145	W14X211	W14X53	W14X145
	4th Story	4516	5961	W14X159	W14X257	W14X53	W14X145
	3rd Story	5161	6813	W14X176	W14X257	W14X53	W14X145
	2nd Story	5806	7664	W14X193	W14X370	W14X53	W14X145
	1st Story	7097	9367	W14X211	W14X370	W14X53	W14X145
9-story	9th Story	1613	2129	W14X109	W14X211	W14X53	W14X132
	8th Story	2903	3832	W14X109	W14X211	W14X53	W14X132
	7th Story	3871	5109	W14X132	W14X211	W14X53	W14X145
	6th Story	4839	6387	W14X176	W14X455	W14X53	W14X145
	5th Story	5484	7239	W14X176	W14X455	W14X53	W14X159
	4th Story	6129	8090	W14X211	W14X455	W14X53	W14X159
	3rd Story	6451	8516	W14X211	W14X605	W14X53	W14X176
	2nd Story	7097	9368	W14X211	W14X605	W14X53	W14X176
	1st Story	7097	9368	W14X233	W14X605	W14X53	W14X176

NUMERICAL MODELING

The numerical modeling and subsequent time history analyses of the frames have been performed using OpenSees (OS) [19]. The details of the modeling of various components of all studied frames are discussed in the following sections.

Modeling of BRBs and FSBRBs

The brace has been modeled using a series of beam-column elements representing different sections of BRBs. Elastic beam-column elements possessing a high moment of inertia have been used to model the non-yielding regions of the brace. Non-yielding region consists of end connection, transition segments, and the elastic HSS element, as shown in Figure 1. The core length (yielding part) and the length of the elastic HSS element of both BRBs have been adjusted accordingly using the calculated areas of the core so that the braces with comparable axial stiffnesses can be used in a particular story for the studied frames. The length of the core element of the steel BRBs and FSBRBs are thus taken as $0.4L_{wp}$ and $0.45L_{wp}$, respectively, where L_{wp} is the work-point to work-point length. The elastic HSS element needs to be adequately designed to avoid global instability of the braces. However, the area of elastic HSS element has been considered as four times the equivalent steel BRB core area for simplicity, which is adequate in providing overall stability to the brace [17]. The end connection and transition segments have been assumed constant for both types of braces having a length equal to $0.24L_{wp}$ and $0.06L_{wp}$, respectively, having cross-sectional areas equal to 3.5 times and 2.5 times the core area of steel BBB [15]. The rigid zone offsets of 0.05 L_{wp} have been assumed at both ends, which are connected (non-moment resisting connection) to either end of the braces.

Force-based beam-column element using fiber sections has been used to capture the nonlinear behavior of the yielding region of the braces. Steel04 uniaxial material available in the OpenSees framework [19] has been used to model the stress-strain characteristics of individual fibers. Steel04 material allows the user to provide different kinematic and isotropic hardening parameters in tension and compression. Also, the ultimate stress option available in the Steel04 material definition can be used to limit the stress increment due to hardening for higher strain which could have otherwise given erroneous results. This is useful, especially for validating the Fe-SMA model, where high initial strain-hardening parameters can generate significantly higher stresses at high strain values. All-steel BRBs tested by Wu et al. [22] have been used to validate the steel BRB model using Steel04 material. Figure 4 (a) compares the numerically estimated results and experimental results of the w160t20-1 specimen tested by Wu et al. [22]. The stress-strain properties for Fe-SMA used in the FSBRB model have been validated using the reduced scale buckling restrained bars tested by Wang et al. [10]. Figure 4(b) shows the comparison between the numerical and experimental stress-strain behavior of Fe-SMA bars tested by Wang et al. [10]. The numerical model used in the analysis was able to capture the hysteretic response of both steel and Fe-SMA with sufficient accuracy.

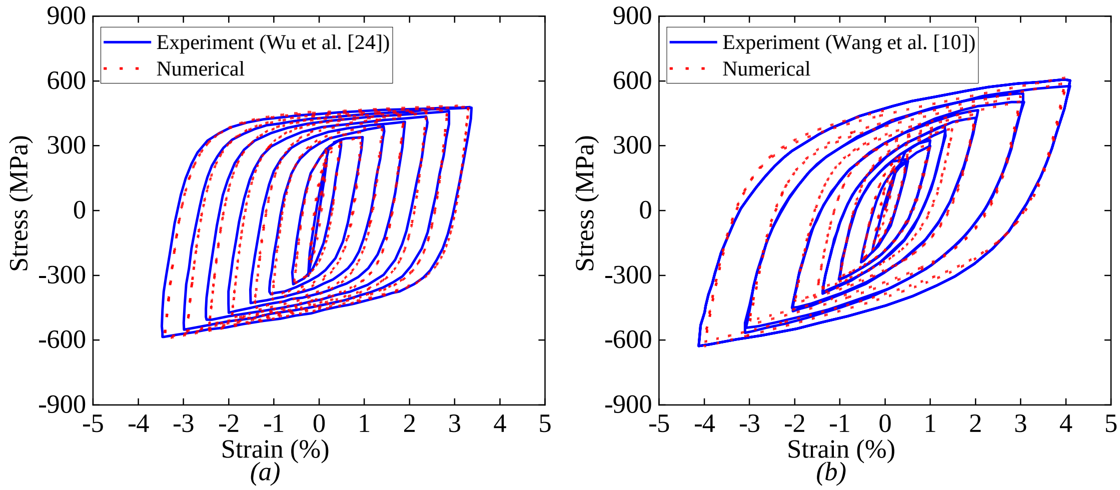

Figure 4. Validation of numerical model with experimental results: (a) Steel BRB, (b) Fe-SMA.

Modeling of Frame Members

The beams and columns have been modeled using force-based beam-column elements with fiber sections at each integration point. Five integration points have been considered in the current study for capturing the overall flexural and axial behavior of members. The hysteretic material model available in OpenSees [19] has been considered to model the stress-strain characteristics of individual fibers. The yield strength and ultimate strength of the steel W-section have been considered as 344 MPa and 448 MPa, respectively, having a post-yield stiffness ratio of 3.7% [12]. The rigid sections at the beam-column ends have been modeled using elastic beam-column elements with high flexural rigidity. All the beam-column connections have been considered to be of non-moment resisting type. Column bases for braced bays have been considered fixed, with pinned bases for gravity columns. A leaning column has been modeled using pinned column base which is rigidly connected to the frame nodes at each level to consider the P-Delta effects. Classical Rayleigh damping of 2% has been considered in the model for the time-history analyses.

Ground motion scaling

The ground motions used in the SAC study [25] has been considered for the nonlinear time history analyses of the frames. The suite consists of a set of 20 ground motions (LA01-LA20) representing the DBE hazard level having a probability of exceedance of 10% in 50 years for Los Angeles. The ground motions have been scaled in such a way that the average of the response spectra of LA01-LA20 ground motions for 5% damped condition is above the target spectrum for the time period ranging between 0.2*T* and 1.5*T*, where *T* is the fundamental period of the structure [21]. Figure 5 shows the scaled mean response spectra for the 3-story, 6-story, and 9-story buildings used in the current study for the DBE hazard level.

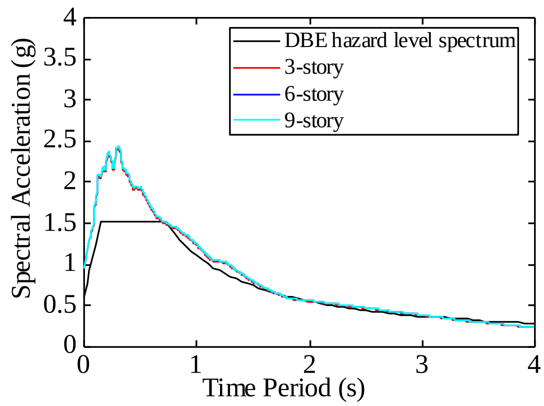

Figure 5. Scaled mean response spectra and target level response spectrum.

ANALYSIS RESULTS

The nonlinear time history analyses have been performed for all six frames to compare the seismic performance of frames designed with FSBRB and steel BRBs. Linear modal analysis has been performed to compare the lateral stiffness of the frames. As shown in Table 2, the fundamental period of all the BRB frames are almost similar to the equivalent FSBRB frames. This ensures that the frames have comparable initial lateral stiffness with different post-yield stiffnesses to compare two different bracing systems better. The two main parameters investigated in the current study are the inter-story drift ratios (ISDR) and residual drift ratios (RDR).

Table 2. Fundamental time period of the frames.

	BRBF	**FSBRBF**
3-story	0.512s	0.507s
6-Story	0.810s	0.803s
9-Story	1.156s	1.148s

The effect of using FSBRB in reducing the residual drifts has been discussed in this section, considering a single ground motion. The inter-story drift responses of BRBF9 and FSBRBF9 frames for scaled LA03 ground motion are shown in Figure 6 at three different story levels (1^{st}, 5^{th}, and roof levels). The observed maximum ISDR at 1^{st}, 5^{th}, and 9^{th} floor levels are 1.41%, 2.26%, and 1.33%, respectively for BRBF9 and 1.36%, 2.27%, and 1.82%, respectively for FSBRBF9. The ISDR values are similar in the first few cycles of loading till the braces in a story start to yield because of designed similar initial stiffnesses of the braces. As the brace starts to yield, the difference in the ISDR can be noticed because of the different post-yield stiffnesses of steel BRB and FSBRB. The maximum ISDR is similar for the lower stories in both cases, with slightly higher values for the upper stories in the case of FSBRBF9. Although, there is a significant difference in the value of RDR, as observed in Figure 6. The RDR of BRBF9 at 1^{st}, 5^{th}, and 9^{th} floor levels are 0.55%, 1.54%, and 0.55%, respectively. These values are minimized to 0.20%, 0.68%, and 0.27%, respectively, using FSBRBs instead of steel BRBs. The percentage reduction in RDR is 45-64% for LA03 ground motion. Figure 7 shows the axial force-deformation hysteretic response of BRB and FSBRB located in the ground story. The low residual deformation of the FSBRB specimen (marked as green) because of high post-yield stiffness supports the observation of a lower RDR value of FSBRBF.

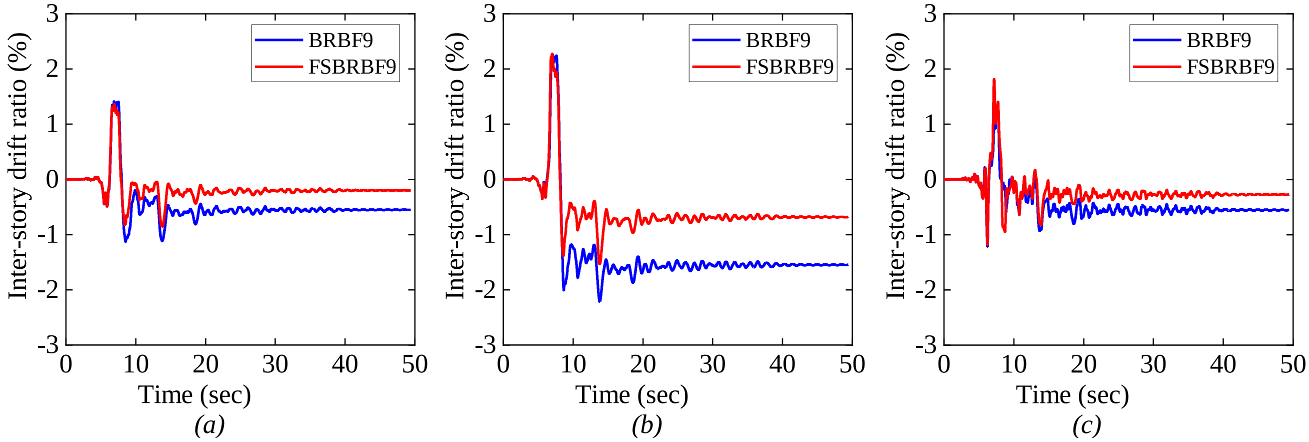

Figure 6. Inter-story drift response of BRBF9 and FSBRBF9 frames at different story levels for LA03 ground motion: (a) Level 1, (b) Level 5, (c) Level 9.

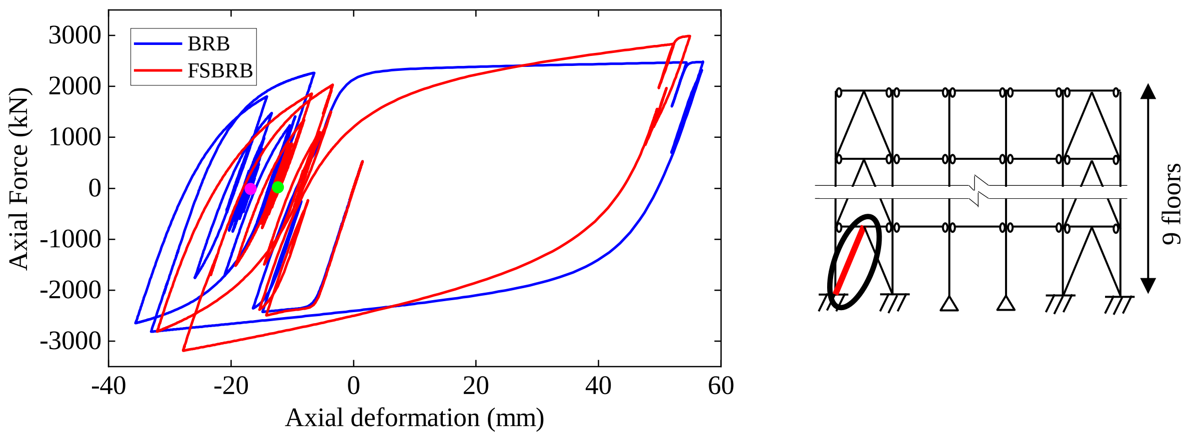

Figure 7. Axial force deformation response of the brace located in the bottom story of BRBF9 and FSBRBF9.

The seismic responses of all the frames for the selected ground motions are presented using the average maximum ISDR and average RDR, as shown in Figure 8 and Figure 9. The average maximum ISDR value for the 3-story frames ranges between 2.20% to 2.89% and 2.04% to 2.95% for BRBF3 and FSBRBF3, respectively (Figure 8 (a)). Higher ISDR values greater than 2% have been observed for both frames. This behavior is due to the higher seismic demand as the scaling method used in the study increased the difference between the mean response spectrum and the target level response spectrum at the fundamental time period of the BRBF3 and FSBRBF3. For the 6-story frames, the average maximum ISDR value ranges between 1.49% to 2.27% and 1.40% to 2.08% for BRBF6 and FSBRBF6, respectively (Figure 8 (b)). Similarly, the average maximum ISDR value ranges between 1.22% to 2.06% and 1.17% to 1.82% for BRBF9 and FSBRBF9, respectively (Figure 8 (c)). For all the studied cases, the observed average maximum ISDRs are similar for BRBF and FSBRBF having equal number of floors. Although, there is a slight increment in the average maximum ISDR values at the upper floors for FSBRBF. This behavior is due to the overstrength of the FSBRBs because of high post-yield stiffness, which prevents the displacement from concentrating at a particular story level, unlike the case of BRBFs, where slightly higher ISDR is observed at lower stories.

The RDR plots representing mean and maximum RDR values observed for a particular story of the frames, as shown in Figure 9, provide a better insight into the advantages of FSBRBs over conventional steel BRBFs, as mentioned earlier. The maximum RDR value for FSBRBF6 is limited to 1.24%, while it exceeds 2% for BRBF6. The maximum observed RDR value for FSBRBF9 for all the ground motions is limited to 1.12%, while it goes up to 1.72% for BRBF9. The higher RDR value tends to concentrate at the intermediate floors for BRBF (BRBF6 and FSBRBF6) and FSBRBFs (FSBRBF9 and BRBF9). The variation of mean RDR values of 3-story frames for different floor levels ranges between 0.46% to 0.61% and 0.24% to 0.30% for BRBF3 and FSBRBF3, respectively (Figure 9 (a)). The mean RDR value ranges between 0.36% to 0.66% and 0.20% to 0.41% for BRBF6 and FSBRBF6, respectively, whereas it ranges between 0.21% to 0.52% and 0.14% to 0.25% for BRBF9 and FSBRBF9, respectively (Figure 9 (b) and (c)). Thus, the mean RDR value of the frames after the replacement with FSBRB reduces from 0.54% to 0.27% for the 3-story frame, 0.56% to 0.33% for the 6-story frame, and 0.42% to 0.22% for 9-story frames. Thus, it shows that the use of FSBRB can lead to a significant reduction in the story drifts at the DBE hazard level.

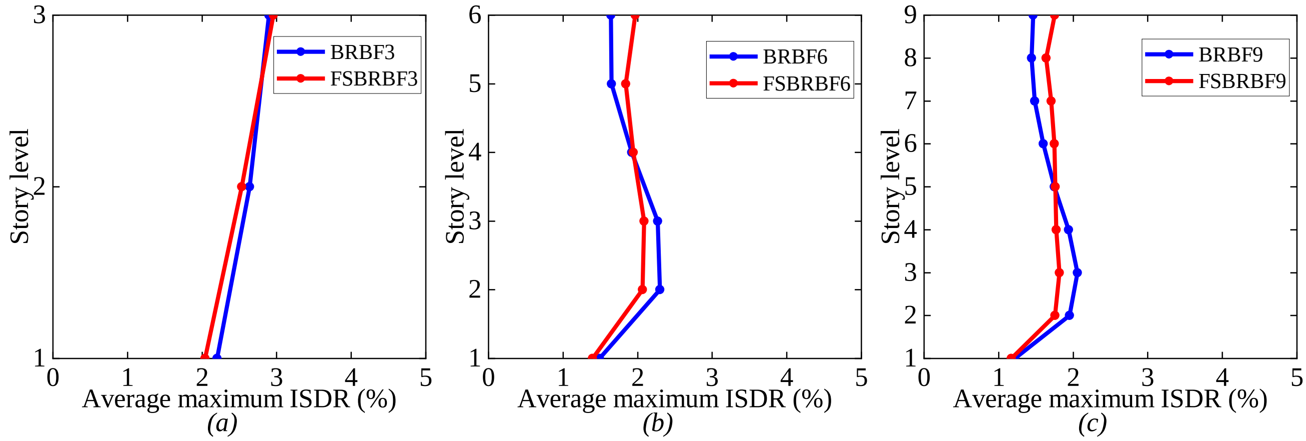

Figure 8. Average maximum inter-story drift ratios of BRBF and FSBRBF: (a) 3-story, (b) 6-story, (c) 9-story.

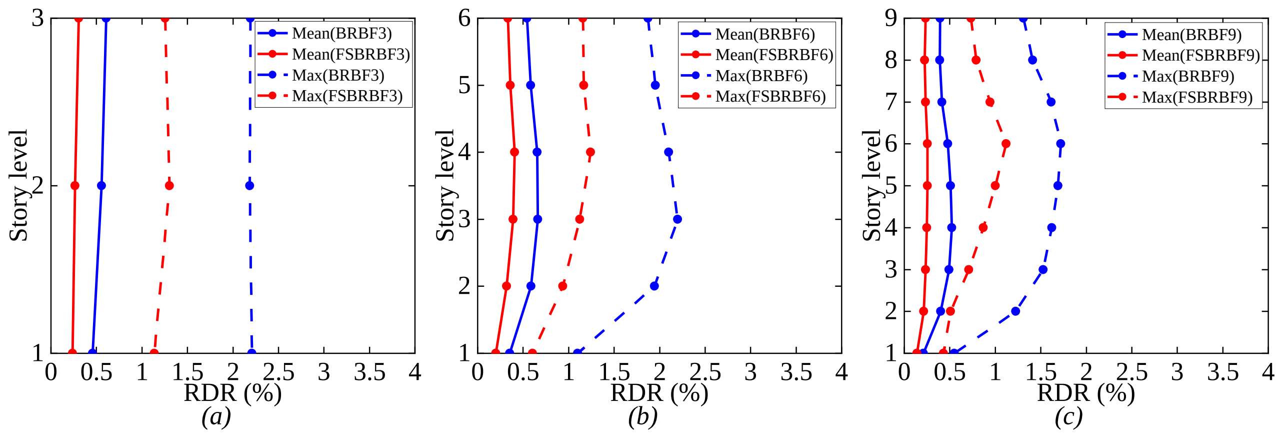

Figure 9. Average residual inter-story drift ratios of BRBF and FSBRBF: (a) 3-story, (b) 6-story, (c) 9-story.

CONCLUSIONS

The current study is focused on the seismic performance assessment of low to medium-rise frames (3-story, 6-story, and 9-story) equipped with Fe-SMA-based buckling restrained braces (FSBRBs). It provides a comparative analysis of parameters like inter-story drift ratios (ISDR) and residual inter-story drift ratios (RDR) of FSBRBFs with frames equipped with conventional steel BRBs having comparable axial stiffnesses. Pinned beam-column connection with fixed column bases (braced bays) has been considered for the analysis using OpenSees. The following conclusions can be drawn from the present study:

- The frames designed with FSBRBs with Fe-SMA as the core element in series with an elastic element provide lateral post-yield stiffness to the entire system, which helps reduce the values of RDR.
- FSBRBF has a similar advantage as conventional steel BRBFs in reducing the ISDR with the added benefit of reduced residual drifts. The observed percentage reductions in the mean RDR values of the FSBRBFs with respect to BRBFs for the selected DBE hazard level ground motions are 50% (3-story), 41% (6-story), and 48% (9-story).
- Thus, FSBRB can be an alternative to conventional steel BRBs as a lateral force-resisting system.

REFERENCES

[1] Watanabe, A., Hitomi, Y., Saeki, E., Wada, A., and Fujimoto, M. (1988). "Properties of brace encased in buckling-restraining concrete and steel tube". In: *Proceedings of Ninth World Conference on Earthquake Engineering (Vol.4)*, Tokyo-Kyoto, Japan.

[2] Tremblay, R., Bolduc, P., Neville, R., and DeVall, R. (2006). "Seismic testing and performance of buckling-restrained bracing systems". *Canadian Journal of Civil Engineering*, 33 (2), 183–198.

[3] Ghowsi, A.F. and Sahoo, D.R. (2015). "Fragility assessment of buckling-restrained braced frames under near-field earthquakes". *Steel and Composite Structures*, 19 (1), 173–190.

[4] Jeffrey, E., Constantin, C., Robert, T., and Hyunhoon, C. (2011). "Residual Drift Response of SMRFs and BRB Frames in Steel Buildings Designed according to ASCE 7-05". *Journal of Structural Engineering*, 137 (5), 589–599.

[5] Macrae, G.A. and Kawashima, K. (1997). "Post-earthquake residual displacements of bilinear oscillators". *Earthquake Engineering and Structural Dynamics*, 26 (7), 701–716.

[6] Kiggins, S. and Uang, C.M. (2006). "Reducing residual drift of buckling-restrained braced frames as a dual system". *Engineering Structures*, 28 (11), 1525–1532.

[7] Xie, Q., Zhou, Z., and Meng, S.-P. (2020). "Behaviour of BFRP tendon systems under cyclic loading and its influence on the dual-tube SC-BRB hysteretic performance". *Construction and Building Materials*, 259, 120388.

[8] Atasever, K., Inanaga, S., Takeuchi, T., Terazawa, Y., and Celik, O.C. (2020). "Experimental and numerical studies on buckling restrained braces with posttensioned carbon fiber composite cables". *Earthquake Engineering and Structural Dynamics*, 49 (15), 1640–1661.

[9] Miller, D.J., Fahnestock, L.A., and Eatherton, M.R. (2012). "Development and experimental validation of a nickel–titanium shape memory alloy self-centering buckling-restrained brace". *Engineering Structures*, 40, 288–298.

[10] Wang, B. and Zhu, S. (2022). "Cyclic behavior of iron-based shape memory alloy bars for high-performance seismic devices". *Engineering Structures*, 252, 113588.

[11] Eatherton, M.R., Fahnestock, L.A., and Miller, D.J. (2014). "Computational study of self-centering buckling-restrained braced frame seismic performance". *Earthquake Engineering and Structural Dynamics*, 43 (13), 1897–1914.

[12] Ghowsi, A.F. and Sahoo, D.R. (2020). "Seismic response of SMA-based self-centering buckling-restrained braced frames under near-fault ground motions". *Soil Dynamics and Earthquake Engineering*, 139, 106397.

[13] Issa, A.S., Haque, A.B.M.R., and Alam, M.S. (2018). "An experimental and numerical investigation of the cyclic performance of a smart self-centering bracing system". In: *6th International Disaster Mitigation Specialty Conference 2018*, Fredericton, Canada.

[14] Ghowsi, A.F., Sahoo, D.R., and Kumar, P.C.A. (2020). "Cyclic tests on hybrid buckling-restrained braces with Fe-based SMA core elements". *Journal of Constructional Steel Research*, 175, 106323.

[15] Pandikkadavath, M.S. and Sahoo, D.R. (2017). "Mitigation of seismic drift response of braced frames using short yielding-core BRBs". *Steel and Composite Structures*, 23 (3), 285–302.

[16] Hoveidae, N., Tremblay, R., Rafezy, B., and Davaran, A. (2015). "Numerical investigation of seismic behavior of short-core all-steel buckling restrained braces". *Journal of Constructional Steel Research*, 114, 89–99.

[17] Hoveidae, N. and Radpour, S. (2021). "A novel all-steel buckling restrained brace for seismic drift mitigation of steel frames". *Bulletin of Earthquake Engineering*, 19 (3), 1537–1567.

[18] Qiu, C., Zhang, A., Jiang, T. and Du, X. (2022). "Seismic performance analysis of multi-story steel frames equipped with FeSMA BRBs". *Soil Dynamics and Earthquake Engineering*, 161, 107392.

[19] Mazzoni S., McKenna F., Scott M.H., and Fenves G.L. (2006). *Open System for Earthquake Engineering Simulation (OpenSees): User Command Language Manual*. Pacific Earthquake Engineering Research (PEER) Center, University of California, Berkeley, USA.

[20] Ohtori, Y., Christenson, R.E., Spencer, B.F., and Dyke, S.J. (2004). "Benchmark Control Problems for Seismically Excited Nonlinear Buildings". *Journal of Engineering Mechanics*, 130 (4), 366–385.

[21] ASCE/SEI 7-16 (2016). *Minimum design loads for buildings and other structures*. American Society of Civil Engineers, Reston, Virginia, USA.

[22] Wu, A.-C., Lin, P.-C., and Tsai, K.-C. (2014). "High-mode buckling responses of buckling-restrained brace core plates". *Earthquake Engineering & Structural Dynamics*, 43 (3), 375–393.

[23] Sahoo, D.R. and Chao, S.H. (2010). "Performance-based plastic design method for buckling-restrained braced frames". *Engineering Structures*, 32 (9), 2950–2958.

[24] ANSI/AISC 341-16 (2016). *Seismic Provisions for Structural Steel Buildings*. American Institute of Steel Construction, Chicago, Illinois, USA.

[25] Somerville, P., Nancy, S., Punyamurthula, S., and Sun, J. (1997). *Development of Ground Motion Time Histories for Phase 2 of the FEMA/SAC Steel Project*. Report No. SAC/BD-97/04, SAC Joint Venture, Sacramento, California, USA.